Ferrari-John, R.S. and Katrib, Juliano and Palade, Paula and Batchelor, A.R. and Dodds, Chris and Kingman, S.W. (2016) A tool for predicting heating uniformity in industrial radio frequency processing. Food and Bioprocess Technology . ISSN 1935-5130

A tool for predicting heating uniformity in industrial radio frequency processing

R.S. Ferrari-John[†], J. Katrib*[†], P. Palade, A.R. Batchelor, C. Dodds, S.W. Kingman

Faculty of Engineering, University of Nottingham, University Park, Nottingham, NG7 2RD, United Kingdom

* Corresponding author. Tel.: +44 (0)115 951 4104

E-mail address: juliano.katrib@nottingham.ac.uk

† Equal contributors

Abstract

Radio frequency energy is utilised for heating in a wide range of applications, particularly in the food industry. A major challenge of RF processing is non-uniform heating in loads of variable and angular geometry, leading to reduced quality and product damage. In the study, the specific effects of geometry on the heating profiles of a range of geometrically variable loads in an industrial scale RF system are analysed, and the understanding used to derive a general tool to predict heating uniformity. Potato was selected as a test material for experimental work; dielectric properties were measured using a 44mm coaxial probe. Analysis of simulated and experimental surface temperature profiles and simulated power uniformity indices indicates that the presence of vertices and edges on angular particles, and their proximity to faces perpendicular to the RF electrodes increases localised heating; faces parallel to the electrodes heated less than those faces perpendicular to them. Comparison of the same geometrical shape in different orientations indicates that overall power absorption uniformity can be better even when localised heating of edges is greater. It is suggested, for the first time, that the rotation of angular shapes within a parallel plate electric field can improve heating uniformity, and that this can be achieved through the design of bespoke electrode systems. A Euler characteristic based shape factor is proposed, again for the first time, that can predict heating uniformity for solid, dielectrically homogenous shapes. This provides industry with a tool to quickly determine the feasibility for uniform RF heating of different three dimensional shapes based on geometry alone. This provides a screening method for food technologists developing new products, allowing rapid assessment of potential heating uniformity and reducing the need for early stage specialist computational modelling.

Keywords

Radio frequency; Industrial heating; Computer simulation; Heating uniformity; Shape factor

1 *Introduction*

Radio frequency (RF) heating has been utilised in a range of research and industrial applications as diverse as wood drying and joining, textiles, composite materials manufacture and most prevalently, the food industry. The literature points to several examples of RF application within the food industry, such as post-harvest pest control (Hou et al., 2016) thermal treatment of vacuum packed foods, (Orsat et al., 2001; Wang et al., 2012), sterilisation and pathogen control (Liu et al., 2011) thawing and tempering (Llave et al., 2014; Uyar et al., 2015) and cooking of comminuted meat products (Laycock et al., 2003).

A variety of different RF electrode configurations are available, dependent on the material to be processed. Staggered through-field electrodes are suitable for processing regular products up to 6 mm thick, whilst stray-field electrodes are used for sheet materials less than 1 mm (Awuah et al., 2014). However, the horizontal electric field patterns generated by these electrode configurations are not suitable for heating thicker materials. Processing of thicker materials is achieved using parallel plate electrodes. This configuration provides a uniform electric field and therefore even heating, provided that the load itself is uniform, both geometrically and dielectrically. This has limited commercial applications for parallel plates to loads of regular geometry, such as slabs of frozen meat, loaves or beds of grain, where uniform heating is achievable. Poor heating uniformity can lead to reduction in product quality (Wang et al., 2005) or in extreme cases thermal damage to the product (Birla et al., 2004).

To apply RF heating to a wider range of industrial heating processes, we need to understand the heating challenges in the treatment of geometrically variable loads. The dielectric properties, chemical composition, internal structural properties and geometry are important considerations for understanding dielectric heating of materials. System parameters such as electrode height and configuration, as well as the positioning of the load between the electrodes, can also influence heating uniformity. An investigation by Romano and Marra (2008) considered the heating of simple shapes in a RF applicator, and showed that for that different shapes in different orientations had different heating uniformity. A recent study by Uyar et al. (2016) indicated that for cubes heated in a small scale parallel plate, the projection area and distance of the load from the electrodes can be varied to improve heating uniformity.

In this work we have built upon the studies above and have developed an experimental approach to assess non uniformity in the RF processing of irregular and geometrically variable loads at industrial scale (1-10 tonne/hr). Our objectives were to evaluate the volumetric RF heating uniformity for a range of geometric loads in an industrial scale system and to use these results to predict potential heating uniformity based on simple geometrically

parameters. To our knowledge, this is the first study to apply numerical modelling to the investigation of heating uniformity in geometric loads in industrial scale systems, underpinned by thermal and dielectric characterisation. The output of this investigation is a tool to predict the heating uniformity of three dimensional solid geometries under equivalent RF processing conditions. Achieving this without complex multiphysics simulations will accelerate development timescales of new food products and potentially widen the scope of industrial RF heating.

2 *Materials and Methods*

2.1 Sample Selection and Preparation

King Edward potato was selected for this investigation as a suitable material from which to fabricate the shapes for the experimental investigation. The selection was based on its structural uniformity, the ease with which it could be formed into a variety of shapes and the homogeneity of its dielectric properties (DPs). It is also a common foodstuff relevant to RF food applications. Baking potatoes (average mass ~250g) were purchased from a local supermarket. The potato was cut into the desired shapes immediately prior to dielectric property measurement and treatment to minimise any oxidation or moisture loss in the samples.

2.2 Physical properties of food material

The dielectric properties of the potato were determined using a 44mm low frequency open ended coaxial probe (National Physical Laboratory, 2015) connected to a network analyser (Agilent 8753ES). Before measurements were conducted, the probe was calibrated using an open/short and reference liquid (ethanol) in sequence (Clarke, 2003). Additionally, methanol was measured to check the calibration. The complex permittivity of three potato samples of 40mm thickness were each measured in triplicate at 20, 40 and 60°C. Samples were placed in an oven at the desired temperature and left for 2 hours to equilibrate.

The mass loss on drying method was used to determine the moisture content of the potato (ASTM, 2014). Eight samples of ~20g each were weighed and then left to dry out in an oven at 105°C for 8 hours. The mass loss of each sample was recorded and the moisture average moisture content of the potato was calculated to be 83.3% ±0.9%. The moisture loss of samples for dielectric property measurement was also quantified. This was to ensure that no significant change in sample moisture content would occur during the course of dielectric property measurement at room temperature. Eight 20mm thick slices of potato (with the skin removed) were left under ambient conditions; the mass of each sample was weighed periodically over 350 minutes. After 350 minutes the average mass loss of samples was shown to be 0.9%, indicating no significant change in moisture content with respect to dielectric property measurements at room temperature over the measurement period. The

residual moisture content of 3 control samples at 40 and 60 °C was also measured using the mass loss on drying method. The density and thermal properties of potato at 20 °C were taken from the ASHRAE Handbook of Refrigeration (2006).

The dielectric and thermal properties of potato and air at room temperature were used in the simulation, see Table 1. The dielectric properties of potato measured at 27.12 MHz and 20°C are comparable to those of other fruit and vegetables of similar moisture contents reported in the literature (Sosa-Morales et al., 2010).

Table 1 Properties of potato and air for modelling

Parameter		Potato	Air
Thermal diffusivity, α	m^2/s	$1.3x10^{-7}$ (a)	$2.2x10^{-5}$ (b)
Specific heat capacity, C_p	J/kg.K	3684.384 (a)	1000 (b)
Density, ρ	kg/m^3	1057 (a)	1.2 (b)
Dielectric loss, ε''	20°C	293.5	0 (c)
Dielectric constant, ε'		48.7	1.0046 (d)
Moisture content, %		83.3	-
Dielectric loss, ε''	40°C	623.4	-
Dielectric constant, ε'		57.2	-
Moisture content, %		79.8	-
Dielectric loss, ε''	60°C	693.0	-
Dielectric constant, ε'		118.2	-
Moisture content, %		73.3	-

(a) (ASHRAE, 2006)

(b) (Toolbox, 2015)

(c) (COMSOL Multiphysics, 2012)

(d) (Katrib et al., 2015)

2.3 Computer Simulation

A computational study was used to assess the thermal profiles observed during experimental RF heating of the test shapes. Often, quasi-static approximations are used in the radio frequency regime for problems involving time dependent electromagnetic fields, in which the spatial distribution of the field is almost the same as the static problem. This approximation is valid for applicator geometries that are small compared to the wavelength, reducing the problem to Laplace's equation, and decoupling the electric and magnetic field in Maxwell's equation. Given that this work studies an entire industrial scale RF processing

system, containing small and geometrically variable loads, the full wave electromagnetic model is simulated.

The RF heating process was modelled using COMSOL Multiphysics software (V5, COMSOL Multiphysics, Burlington, USA), a commercially available software based on the finite element method (FEM). In this study, the RF electromagnetic module was coupled to the heat transfer module to simultaneously solve EM and heat transfer equations.

2.3.1 Physical model

The Sairem 50 Ω RF system used in the experimental work and modelled in the computational study comprised a 27.12 MHz 20kW generator providing electromagnetic energy via coaxial line to an applicator, with a series of inductor and capacitors to allow impedance matching. A pair of parallel plate metal electrodes forms the cavity, and applies a uniform electric field to the load when the system is in operation. Figure 1 illustrates the system.

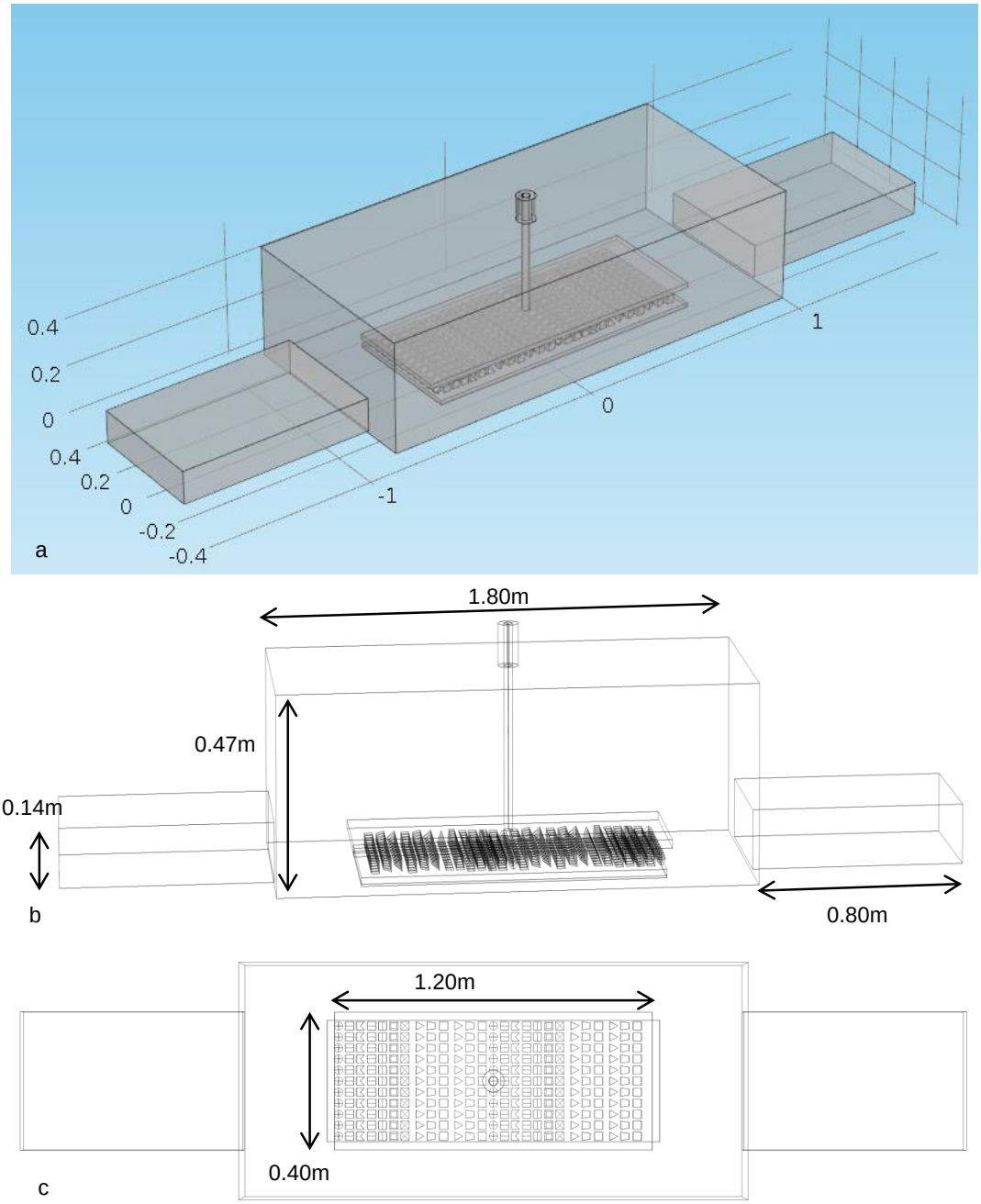

Figure 1 (a) 3D Scheme 50 Ω 20 kW 27.12 MHz RF system and material load (b) cavity and choke dimensions (c) electrode dimensions

The power dissipation density in a material due to radio frequency heating is a function of internal electric field strength within the material, the frequency of the radio frequency radiation and the dielectric properties of the material. For a uniform electric field, this is given by Equation 1 (Metaxas and Meredith, 1983).

$$P_d = \omega \varepsilon_0 \varepsilon'' E^2 \tag{1}$$

Where P_d is the power dissipation density (W/m^3); ω is $2\pi f$ (rad/s) f is the frequency of applied electromagnetic energy (Hz); ε_0 is the permittivity of free space (8.854x10^{-12} F/m); ε'' is the dielectric loss factor; E is the electric field strength in the material (V/m).

2.3.2 Governing equations

The governing electromagnetic wave equation for the time-harmonic and eigen frequency problems solved by Comsol is given by Equation 2.

$$\nabla \times \mu_r^{-1}(\nabla \times \bar{\mathbf{E}}) - k_0^2 \left(\varepsilon_r - \frac{j\sigma}{\omega \varepsilon_0}\right) \bar{\mathbf{E}} = 0 \quad (2)$$

Where μ_r is the relative permeability of the material; $\bar{\mathrm{E}}$ is the electric field strength (vector); k_0 is the wave number of free space (rad/m); ε_r is the relative permittivity of the material; σ is the conductivity of the material (S/m); j is the $\sqrt{-1}$; ω is the angular frequency of the wave (rad/s); ε_0 is the permittivity of free space (8.854x10^{-12} F/m).

The governing heat transfer equation in the electromagnetic field is described by Equation 3:

$$\rho C_p u.\nabla T = \nabla.(k\nabla T) + Q \quad (3)$$

There ρ is the density of the material (kg/m^3), velocity field (m/s), C_p is the specific heat of the heated material (J kg^{-1} K^{-1}), T is the temperature inside the material (°C), k is thermal conductivity (W m^{-1} K^{-1}), and Q is the total electromagnetic heating losses (W/m^3).

The heat transfer model incorporated conduction within the load and heat generation due to RF heating. The total electromagnetic heating losses are defined as the combination of the resistive and magnetic losses, as shown in Equations 4 to 6.

$$Q = Q_{rh} + Q_{ml} \quad (4)$$

$$Q_{rl} = \frac{1}{2} Re(J.E^*) \quad (5)$$

$$Q_{ml} = \frac{1}{2}\, Re(i\omega B.H^*) \quad (6)$$

Where Q_{rl} is the resistive loss; Q_{ml} is the magnetic loss; J is current density (A/m^2); E^* is the electric field strength (V/m); B is the magnetic flux density (T); H^* is the magnetic field strength (A/m).

In the model, the electromagnetic heating module combined the features of the electromagnetic wave frequency domain interface with that of the heat transfer interface. The interaction defined in equation 3 sets the electromagnetic losses as sources for the heat transfer equation. The basis of this interface is the adiabatic assumption that the electromagnetic cycles time is short compared to the thermal timescale.

2.3.3 Initial and boundary conditions

A scattering boundary condition was used for the chokes of the tunnel, with the exits being transparent to a scattered wave. The boundary condition is also transparent for incoming and outgoing (scattered) plane waves. The input power was modelled as lumped coaxial port with an input of 2.9 kW (equivalent to that used in experimental heating trials) connected to two parallel plate electrodes defined as 'structural steel' inside a large rectangular metallic enclosure. A more detailed commentary of the use of boundary conditions in computational modelling of RF systems is available in Uyar et al. (2016) and COMSOL Multiphysics (2012).

The space between the two electrodes formed a cavity that filled with the electromagnetic field during operation. The potato material was placed on the bottom (ground) electrode. The tunnel was assumed to have a thermally insulated boundary condition. The initial temperature of the material in the cavity was set to room temperature (18°C). The dielectric material in the cavity was heated due to the conversion of electromagnetic energy to heat. The potato blocks were modelled as per the measured dielectric properties at 27.12 MHz.

An extremely fine tetrahedral mesh (10 elements per wavelength) was generated in the potato sample to improve the accuracy of temperature distribution simulation. Other parts of the system model were constructed with a tetrahedral mesh size of 5 elements per wavelength. The model consists of 1217791 elements. The time steps used in this study were set as 0.5 s. The simulation was run on an Intel workstation with eight Dual Core 2.5 GHz Xeon processors, 192 GB RAM with a Microsoft Windows 7 64 bit operating system.

2.3.4 Power uniformity index

The surface temperature profiles of the modelled shapes were analysed following simulated heating to determine maximum and average temperature rise. In addition, a power uniformity index (PUI) was used to evaluate the uniformity of the electric field within the body of the heated shapes, as proposed previously by Tiwari et al. (2011). The average power density in an RF heated material can be defined as the volume integral of the RF power density divided by the volume of the material, as shown in equation 8. The PUI is then defined as in Equation 9. A value of 1 represents the poorest uniformity; the closer the value is to 0, the more uniform the power absorption.

$$Q_{av} = \frac{1}{\boldsymbol{V_{vol}}} \int_{\boldsymbol{V_{vol}}} Q dV_{vol} \tag{7}$$

$$PUI = \frac{\frac{1}{Vvol}\iiint_{Vvol} sqrt((Q - Qav)^2) dVvol}{Qav} \quad (8)$$

2.4 RF heating experiments

A 20kW Sairem 50 Ω RF system, operating at 27.12 MHz in batch mode was used for heating trials. Prior to RF heating, the test shapes were imaged using a NEC-AVIO H2640 infra-red thermal imaging camera to determine their pre-treatment surface temperature. The emissivity of the camera was set to 0.99 as the temperature of the target object and the surroundings were both close to room temperature (Saunders, 2004). The test shapes were then conveyed into the RF applicator and were treated at 3.0 kW applied power for 10s, with a 60 mm electrode spacing. Once heated, the test material was conveyed out of the RF applicator and aerial thermal images were then captured for 10s after the end of RF treatment.

In the experiment, it was not possible to image all sides of the tests shapes simultaneously. Therefore, thermal image analysis was performed on selected faces of the test shapes to provide a basis for comparison with the COMSOL models. Figure 2 illustrates the faces analysed in both COMSOL and experimentally. In the experiment thermal images were taken pre and post RF treatment of the top surface of each shape, with the exception of the test polyhedron in orientation 3 which was flipped following RF heating to image the underside. Average temperatures were determined in both the computer simulations and experimentally. Temperature rises were then calculated by deducting the average temperature of each of the test shapes prior to RF treatment. Average temperatures corresponded to the mean of the temperatures of each pixel, for each face analysed. All thermal image analysis was carried out using RC Radiometric Complete, a commercially available thermal imaging software (Radiometric Infrared Solutions, 2011).

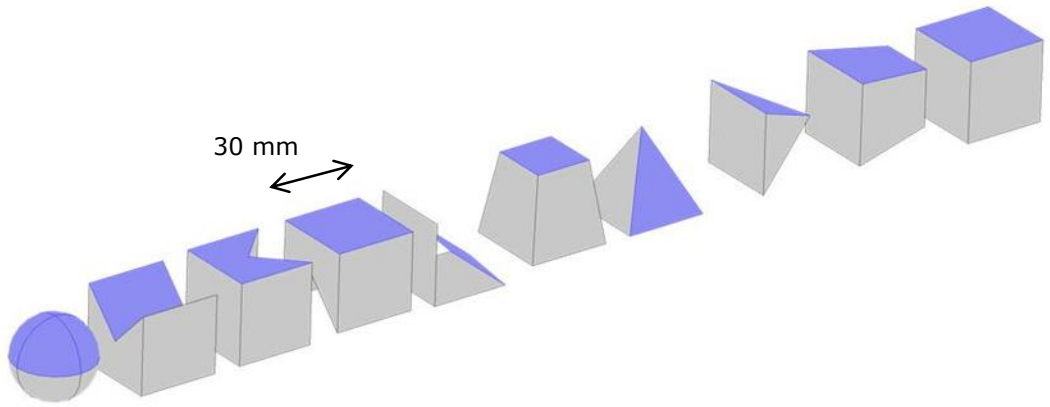

Figure 2 3D Test shape faces chosen for experimental and simulation thermal image analysis

3 *Results and Discussion*

3.1 Simulated temperature profiles

A range of test shapes were both tested experimentally and modelled to provide a means of understanding the effect of geometry on heating uniformity. The cube and sphere represent shapes commonly found in RF heated food products. The pyramid and truncated pyramid were studied to provide further insight into heating profile development. The test polyhedron was designed specifically to test understanding of effects of geometry on the heating profiles. Figure 4 shows the simulated surface temperature profiles of the test shapes following 10s RF heating at 2.9kW applied power, with a 60mm electrode spacing and an initial temperature of 20°C. For the cube, temperatures are highest at the edges and vertices. The cube (Figure 3a) exhibits increased heating on the edges and corners compared to the faces; however heating is greater on the faces that are perpendicular to the electrodes compared to those that are parallel to the electrodes. The sphere (3b) exhibits the lowest but also the most uniform heating. In the case of the pyramid, the highest heating was observed on the tip of the pyramid, both in its primary orientation (3c) and when rotated (3d). The truncated pyramid (3e) shows less heating on the uppermost face compared to the sides. Significantly, it is observed that heating is less this top face than on the surrounding edges, with the centre of the face absorbed less power. The experimental test polyhedron gives insight into how the electric field interacts with the material in the 4 different orientations (3g-3j). The test polyhedron experiences equivalent heating in 3g and 3h, with increased heating on the angled edges nearest to either the top or bottom electrodes. This is expected as these orientations are analogous. As with the cube, it is also evident that the centre of the square face heats less than the edges adjoining that face. In orientation 3j, the test polyhedron also shows heating at the interface between the two angled faces. In general for all the shapes modelled, edges adjoined by faces that are angled with respect to the field lines and the electrode have the greatest power density absorbed, and undergo the greatest heating.

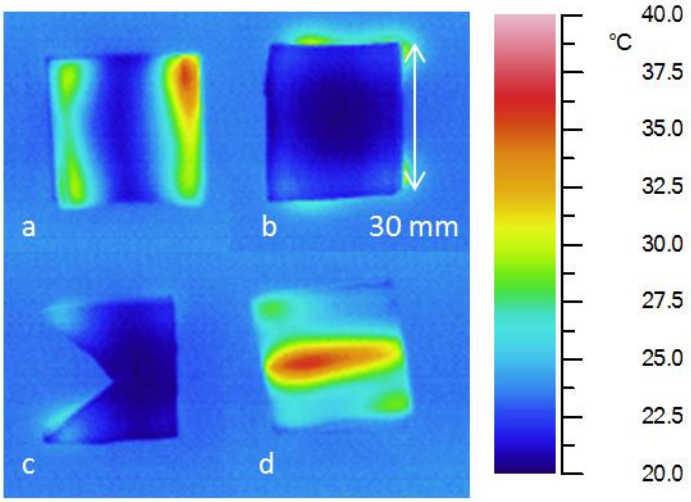

Figure 3 Experimental surface thermal profiles of test polyhedron heated in different orientations (a,b,c,d)

The experimental surface thermal profiles of the test polyhedron heated in four different orientations is shown in Figure 4. It should be noted that 4d was heated as the simulation case in Figure 3j, and then rotated prior to thermal measurement in order to obtain thermal images of the interface of the two angled faces. Comparisons can be made between the thermal images in Figure 5a-5d with the analysed faces in Figure 3g-3j. Both 3g and 4a show increased heating on the upper facing edges. Similarly, both 3h and 4b show minimal heating on the upper square face, the lowest heating being in the centre of the face. 3i and 4c both show increased heating on the triangular edges, although heating is lower in the experimental case. Finally, in both 3j and 4d, there is heating at the interface between the two angled faces. In both the simulated and experimental cases it is noted that he presence of tips and edges on angular particles, and their proximity to faces perpendicular to the RF electrodes increases localised heating. Furthermore faces parallel to the electrodes heat less than those faces perpendicular to them.

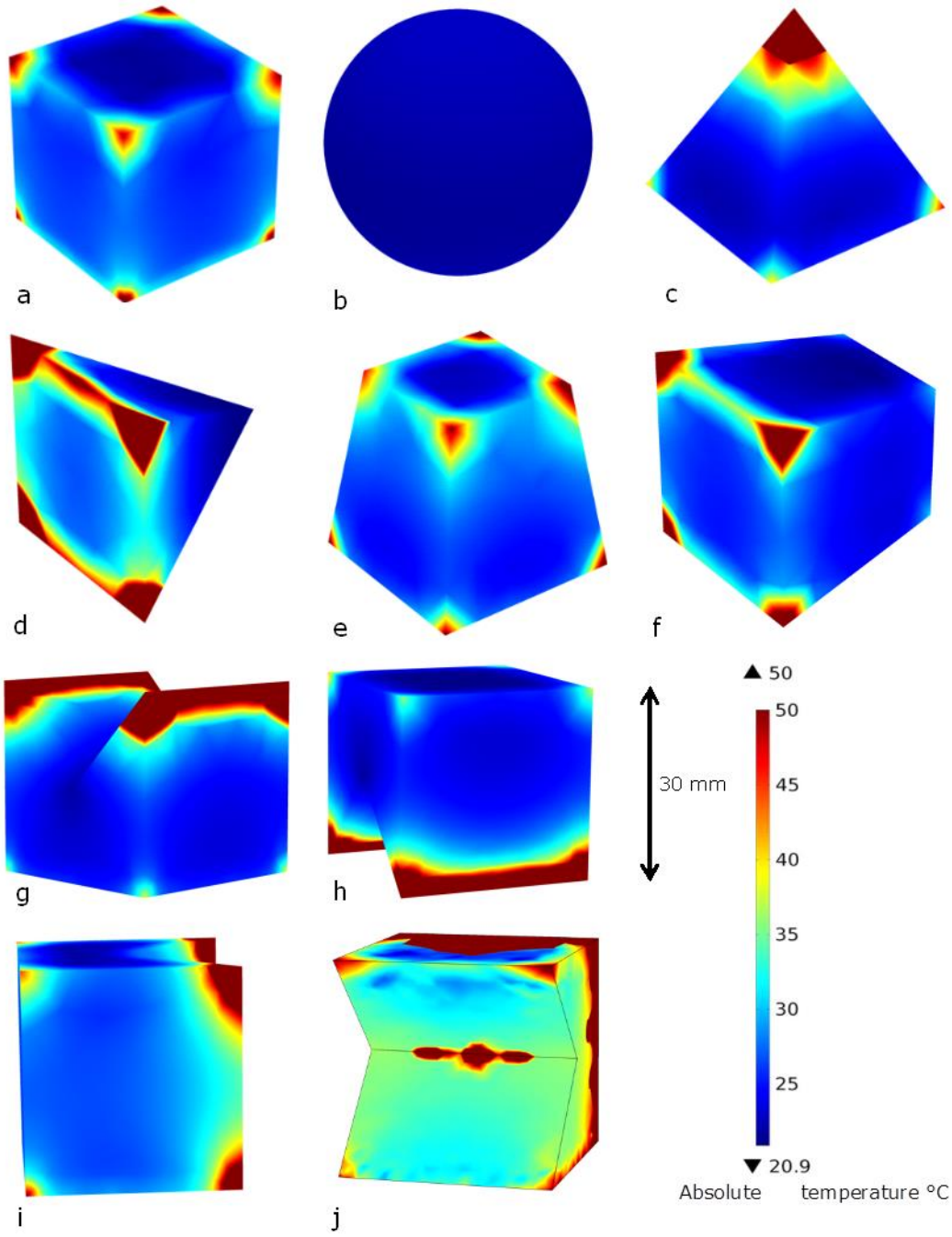

Figure 4 Simulated temperature profiles of test shapes (30mm height) after 10s RF heating, 2.9kW, 60mm electrode spacing, initial temperature 20°C

There is qualitative agreement between the average temperature rise in simulation and experimental cases, as shown in Figure 5, providing validation of the effectiveness of the model. As the purpose of the model was to investigate the influence of load geometry on heating uniformity, this agreement is sufficient. Differences between the simulation and experimental results can be attributed to two main factors. Firstly, heat loss will have occurred during the 10s delay between the end of RF heating and thermal imaging, leading to a significant reduction in measured temperatures in the experimental results. One of the

possible reasons is that during RF heating, water may have been removed from the structure, leading to a significant change in dielectric properties due to both free and bound water content. Given that the goal of this work was to investigate heating uniformity of an array of different geometries in industrial scale systems, a convection cooling model was outside of scope. Future work investigating uniformity in single geometries in smaller electrodes could incorporate coupled moisture changes and convective cooling with the electromagnetic model would lead to much closer agreement between experimental and simulated average temperatures.

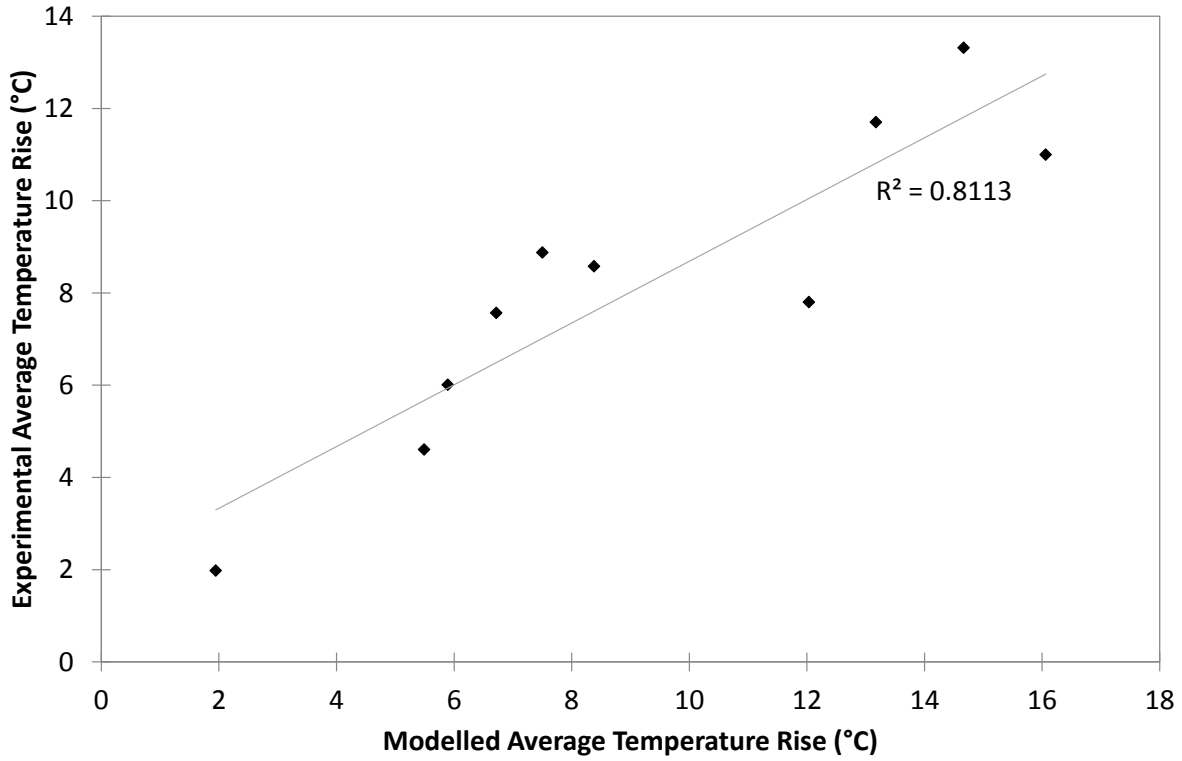

Figure 5 Comparison of simulation and experimental average temperature for analysed faces of shapes

3.2 Predicting heating non-uniformity

Modelling results were used to determine the influence of load shape on heating uniformity. The power uniformity indices were calculated volumetrically for each of the test shapes in each of the heating orientations, as shown in Table 2. The sphere exhibited the best heating uniformity, with a PUI of 0.0693. This can be attributed to the lack of interaction of the material with the electric field, whereby the material distorts the electric field due to the difference in dielectric constant compared to air. This effect has been studied elsewhere in the literature (Jiao et al., 2014). As the sphere has no edges or vertices, there are no field concentrations. The cube exhibits the least uniform heating, with a PUI of 0.7357. It can also be noted that the same shape, for example the polyhedron, has different uniformity values

depending on the orientation in which it is heated, varying for 0.4480 to 0.6509. This is due to different interactions with the electric field in the different heating orientations.

Table 1 PUI and shape factor values of modelled shapes

Shape	Figure 4	PUI	Shape factor
Cube	a	0.7357	0.1300
Sphere	b	0.0693	0.0049
Pyramid	c	0.2320	0.0526
Pyramid	d	0.2966	
Truncated Pyramid	e	0.5681	0.1155
Truncated Pyramid	f	0.4297	
Polyhedron	g	0.4480	0.1184
Polyhedron	h	0.4508	
Polyhedron	i	0.6509	
Polyhedron	j	0.5670	

Previous work has shown that load surface area and volume both influence heating uniformity (Romano and Marra, 2008; Uyar et al., 2016), whilst the results obtained is this work show that vertices and edges lead to field concentrations and increased heating. To describe the geometry of a solid shape in an industrially meaningful way, a shape factor has been developed, based on modification of the Euler characteristic. Euler's polyhedron formula yields a number describing the structure of solid polyhedra, according to the number of vertices, edges and sides. Based on this, a shape factor has been defined that is a function of the geometry and is independent of the size of the shape. The formula for the shape factor is given in Equation 10.

$$Shape\ factor = \frac{(v + e + f)V}{A} \qquad 9)$$

Where v is the number of vertices; e is the number of edges; f is the number of faces; V is the volume; A is the surface area.

In Figure 6, the averaged power uniformity indices for each shape in its different orientations are plotted as a function of its shape factor. The data suggests a clear trend where heating uniformity improves with an increase in shape factor. From this shape factor, it should be possible to predict how uniformly a particular three dimensional geometry will heat in a parallel plate system, without conducting costly RF heating trials or computational studies. This tool is crucial for industry to assess the heating uniformity of novel products without the need for extensive numerical modelling and experimental trials.

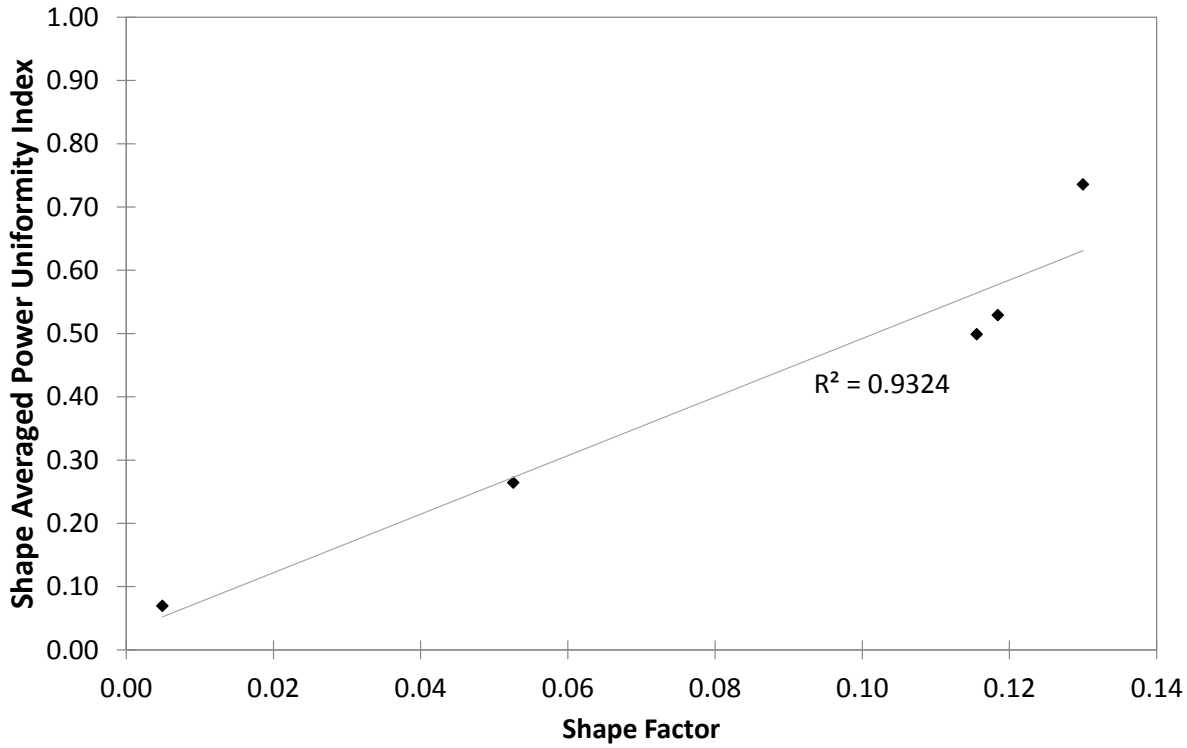

Figure 6 Shape averaged PUI as a function of derived shape factor

Whilst shape factor can be used to predict uniformity, to increase the potential applications for RF heating, methods need to be developed to allowing processing of more angular and irregular shapes. The variation of PUI values obtained for the same shape heated in different orientations suggest that changing the orientation with respect to the electric field during treatment, for example by rotating the load, could lead to an improvement in heating uniformity. This can be visualised as bringing the average shape occupied in space over the RF treatment time closer to that of a sphere, which has the best overall heating uniformity. An alternative way to achieve this without moving the material being heated may be to use successive pairs of electrodes that are offset. In this way, the material could pass through electric fields of different orientations, thereby approximating the rotating of the load within a conventional parallel plate type electric field. Overall, it is suggested that the design of bespoke electrode systems tailored to the geometry of the load provides an opportunity for new commercial applications for RF heating.

4 *Conclusions*

The major challenge for RF processing technologies is non-uniformity in heating, resulting in reduction in product quality in commercial applications. This work focussed on understanding the influence of load geometry on heating uniformity, based on the results of experimental and computational studies of the heating profiles. Test shapes were heated at 3kW in a 27.12 MHz 50 Ω parallel plate RF system in different orientations, with good qualitative agreement between experimental and modelled surface thermal profiles.

The model was used to study the power absorption uniformity of the shapes. The sphere exhibited the best heating uniformity whilst the cube was the least uniform. Different PUI values were obtained when the same shape was heated in different orientations. It is suggested that rotating angular shapes within a uniform electric field, or using bespoke electrodes such as multiple pairs or new geometries, could allow a wider range of materials to be processed using RF technologies.

A new shape factor was proposed that can be used to describe the geometry of shapes. Comparison of shape average PUI values with this shape factor shows that it is possible to predict heating uniformity of homogenous three dimensional loads in industrial scale parallel plate systems based solely on simple geometric parameters. Further computational validation of the shape factor against existing commercial applications and for heterogeneous materials will make this a valuable tool for a wide range of industries.

Acknowledgements

The authors would like to thank the National Physical Laboratory for the loan of their low frequency coaxial probe for dielectric measurements at radio frequencies.

5 *References*

ASHRAE, (2006). ASHRAE Handbook - Refrigeration (I-P Edition). American Society of Heating, Refrigerating and Air-Conditioning Engineers, Inc.

ASTM, (2014). Standard Test Method for Determining Moisture in Raw and Spent Materials.

Clarke, B., (2003). *A Guide to the Characterisation of Dielectic Materials at RF and Microwave Frequencies*. Institute of Measurement and Control.

COMSOL Multiphysics, (2012). 4.3 User's Guide. Comsol.

Hou, L., Johnson, J.A., Wang, S., (2016). Radio frequency heating for postharvest control of pests in agricultural products: A review. Postharvest Biology and Technology 113, 106-118.

Huang, Z., Marra, F., Wang, S., (2016). A novel strategy for improving radio frequency heating uniformity of dry food products using computational modeling. Innovative Food Science & Emerging Technologies 34, 100-111.

Jiao, Y., Tang, J., Wang, S., (2014). A new strategy to improve heating uniformity of low moisture foods in radio frequency treatment for pathogen control. Journal of Food Engineering 141(0), 128-138.

Katrib, J., Folorunso, O., Dodds, C., Dimitrakis, G., Kingman, S.W., (2015). Improving the design of industrial microwave processing systems through prediction of the dielectric properties of complex multi-layered materials. Journal of Materials Science 50(23), 7591-7599.

Laycock, L., Piyasena, P., Mittal, G.S., (2003). Radio frequency cooking of ground, comminuted and muscle meat products. Meat Science 65(3), 959-965.

Liu, Y., Tang, J., Mao, Z., Mah, J.-H., Jiao, S., Wang, S., (2011). Quality and mold control of enriched white bread by combined radio frequency and hot air treatment. Journal of Food Engineering 104(4), 492-498.

Llave, Y., Terada, Y., Fukuoka, M., Sakai, N., (2014). Dielectric properties of frozen tuna and analysis of defrosting using a radio-frequency system at low frequencies. Journal of Food Engineering 139(0), 1-9.

Metaxas, A.a., Meredith, R.J., (1983). *Industrial microwave heating*.

National Physical Laboratory, (2015). Coaxial Sensors for SAR.

Orsat, V., Gariépy, Y., Raghavan, G.S.V., Lyew, D., (2001). Radio-frequency treatment for ready-to-eat fresh carrots. Food Research International 34(6), 527-536.

Radiometric Infrared Solutions, (2011). Radiometric Complete 5.1 Manual

Romano, V., Marra, F., (2008). A numerical analysis of radio frequency heating of regular shaped foodstuff. Journal of Food Engineering 84(3), 449-457.

Saunders, P., (2004). Non-Contact Temperature Measurement in the Food Industry. Measurement Standards Laboratory of New Zealand,.

Sosa-Morales, M.E., Valerio-Junco, L., López-Malo, A., García, H.S., (2010). Dielectric properties of foods: Reported data in the 21st Century and their potential applications. LWT - Food Science and Technology 43(8), 1169-1179.

Tiwari, G., Wang, S., Tang, J., Birla, S.L., (2011). Analysis of radio frequency (RF) power distribution in dry food materials. Journal of Food Engineering 104(4), 548-556.

Toolbox, E., (2015). The Engineering Toolbox.

Uyar, R., Bedane, T.F., Erdogdu, F., Koray Palazoglu, T., Farag, K.W., Marra, F., (2015). Radio-frequency thawing of food products – A computational study. Journal of Food Engineering 146(0), 163-171.

Uyar, R., Erdogdu, F., Sarghini, F., Marra, F., (2016). Computer simulation of radio-frequency heating applied to block-shaped foods: Analysis on the role of geometrical parameters. Food and Bioproducts Processing 98, 310-319.

Wang, J., Luechapattanaporn, K., Wang, Y., Tang, J., (2012). Radio-frequency heating of heterogeneous food – Meat lasagna. Journal of Food Engineering 108(1), 183-193.